Experimental Examination of the Leading-Edge Suction Analogy

Joseph Er-El* and Zohar Yitzhak†
Technion—Israel Institute of Technology, Haifa, Israel

The potential and vortical components of the normal force and their chordwise distribution, as defined by the Leading-Edge Suction Analogy (LESA), as well as the normal force itself and its chordwise distribution, were obtained experimentally and were compared with the predicted results. The comparison was carried out for the delta wings having leading-edge sweep angles of 75 and 60 deg. The experimental results were obtained from surface pressure measurements by invoking the linearized potential-flow wing theory, which was also used in the derivation of LESA. The comparison shows that, for the low-aspect-ratio wing, the agreement between measured and predicted results is good—in the 0–20 deg incidence range. In the high-aspect-ratio wing, the differences between experiment and theory are large for C_{NP}, C_{NV}, and their longitudinal loadings, and considerably smaller for C_N. Thus, LESA appears less valid for the high-aspect-ratio wing than was previously thought on the basis of a comparison of the C_N values only.

Nomenclature

A = wing area
AR = aspect ratio
c = wing root chord
C_N = normal force coefficient $= N/q$
C_n = longitudinal loading of C_n
C_{NP} = potential component of C_N
C_{np} = longitudinal loading of C_{NP}
C_{NV} = vortical component of C_N
C_{nv} = longitudinal loading of C_{NV}
C_p = pressure coefficient
C_{sp} = leading-edge suction force coefficient
N = normal force
q = dynamic pressures
$s(\bar{x})$ = wing local semispan
$\bar{x}$ = nondimensional chordwise coordinate $= x/c$
$\bar{y}$ = nondimensional local spanwise coordinate $= y/s(\bar{x})$
α = angle of attack

Superscripts

l = lower surface of the wing
u = upper surface of the wing

Subscripts

0 = measured at $\alpha = 0$ deg
$[\ ]_{np}$ = contribution of the term in the square brackets to C_{np}

Introduction

THE Leading-Edge Suction Analogy (LESA) is the basis of an analytical method of predicting the low-speed lift characteristic of delta wings. It was proposed by Polhamus[1-3] in 1966 and has been in wide use ever since. The predictions are in good agreement with experimental results for wings having aspect ratios of less than 2 and angles of attack of 0–20 deg. According to this method, the normal force, C_N, is assumed to be a superposition of a potential component C_{NP} and a vortical component C_{NV}.

$$C_N = C_{NP} + C_{NV} \tag{1}$$

Received May 19, 1985; revision received Feb. 7, 1987. Copyright © American Institute of Aeronautics and Astronautics, Inc., 1987. All rights reserved.

*Senior Lecturer, Department of Aeronautical Engineering.
†Graduate Student; currently at the University of Southern California, Los Angeles, CA.

The expressions for C_{NP} and C_{NV} are derived in Ref. 1. C_{NP} is given by

$$C_{NP} = K_p \sin\alpha \cos\alpha \tag{2}$$

where K_p is determined by linearized potential-flow wing theory. C_{NV} is assumed to be equal to the leading-edge suction C_{sp}, and is given by

$$C_{NV} = C_{sp} = K_V \sin^2\alpha \tag{3}$$

K_V is determined from the leading-edge suction calculation.[1]

Comparisons of the predicted normal forces with measurements were carried out by Polhamus[1] and Wentz and Kohlman[4] for delta wings of aspect ratios ranging from 0.5 to 4. Very good agreement was observed in the 0–20-deg incidence range, especially in the lower-aspect-ratio wings. At higher aspect ratios, the analogy predicts somewhat higher C_N values than the experimental results.

LESA was also used by Snyder and Lamar[5] to predict the longitudinal distribution of C_{NP}, C_{NV}, and C_N. The predicted C_N distributions were shown to be in good agreement with experimental results for a delta wing of aspect ratio near 1 in the angle-of-attack range of 0–30 deg.

The good agreement between the LESA predictions and the experimental results as well as simplicity in the use of the analogy have made it a widely used tool both in engineering applications and in the evaluation of higher-order numerical methods of delta wing aerodynamics. However, the comparison between the predicted and experimental results was done, in the previously mentioned studies, only for the normal force and not for its potential and vortical components. It is of interest, therefore, to extend the comparison to the potential and vortical components and their longitudinal distributions.

The purpose of the present study is to obtain $C_{np}(\bar{x})$, C_{NP}, $C_{nv}(\bar{x})$, and C_{NV} experimentally, analyze them, and compare them with the values predicted using the LESA method.

Materials and Methods

The difficulty (or, probably the impossibility) of the direct measurement of C_{NP}, C_{NV}, and their longitudinal loadings required the use of a different method to determine them experimentally. The method devised here was based on pressure measurements on the upper and lower surfaces of the delta wing.

The surface pressures used in this study were measured on two sharp-edged thin delta wings, with no camber, having

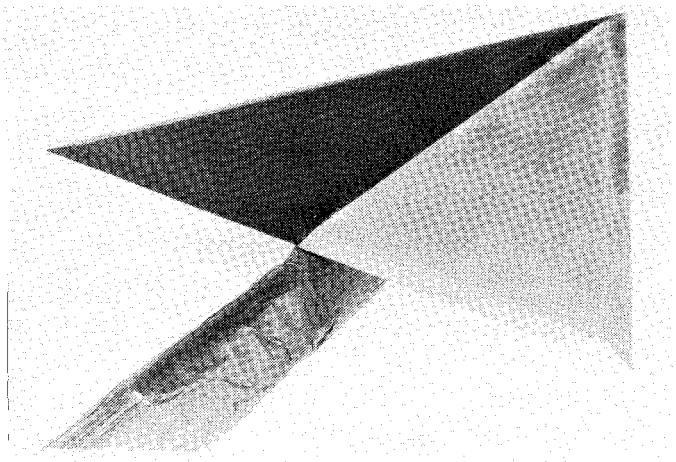

Fig. 1 Typical wing model (the model shown is the 60-deg swept wing).

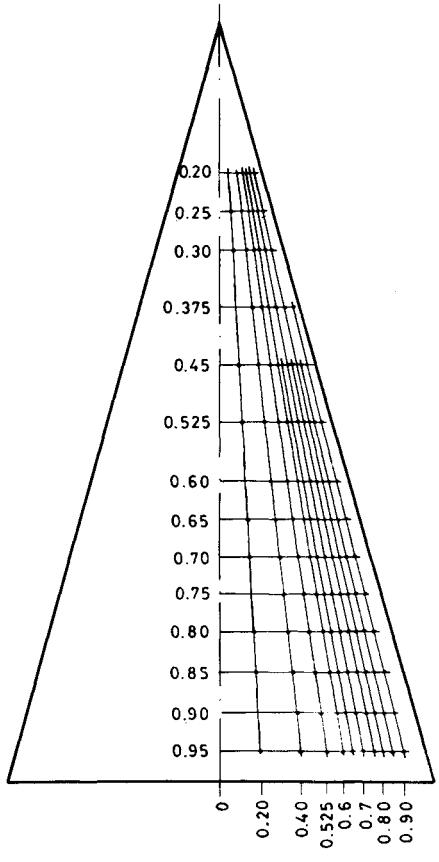

Fig. 2 Map of the pressure holes on the 75-deg sweep delta wing.

leading-edge sweep angles of 75 and 60 deg (aspect ratios of 1.07 and 2.31, respectively). The root chord lengths of the wings are 246 and 302 mm, respectively; the thickness of each wing is 3 mm. Each of these wings has two flat surfaces and symmetrical wedge-shaped (30-deg apex angle) leading and trailing edges. The wingholder (used in both wings) is a vertical strut connected to the lower surface, leaving the pressure measurement surface free of obstructions (Fig. 1). The tests were carried out at an airspeed of 32 m/s. The pressures on each surface were measured in an array of pressure taps (130 in the low-aspect-ratio wing and 128 in the other) located at the junctions of 10 rays, emanating from the wing apex, and 14 spanwise rows (Figs. 2 and 3).

The pressure measurement system is based on three 48-port scanivalve modules, each connected to a membrane-

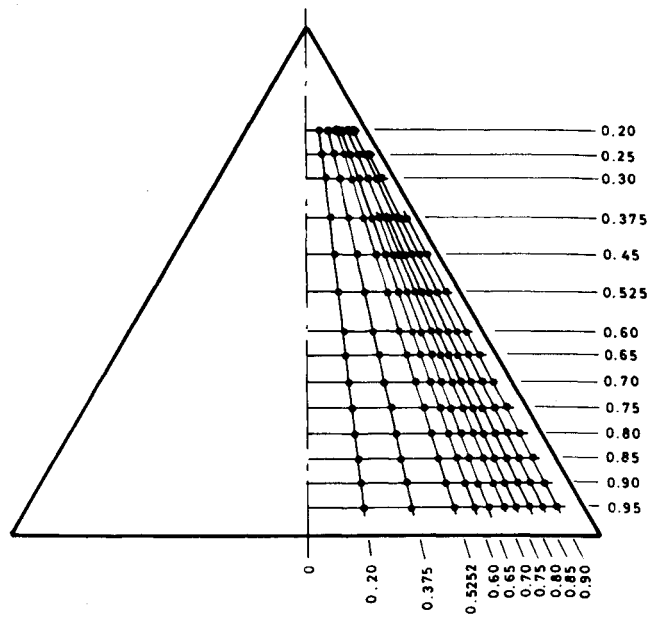

Fig. 3 Map of the pressure holes on the 60-deg sweep delta wing.

type pressure transducer. In a typical experiment, the wing was set at a prescribed angle of attack, and pressure measurements were taken on the upper surface. The wing was then turned over so that the pressure measurement surface became the lower surface, and the data acquisition procedure resumed. A detailed description of the models and the instrumentation is given in Refs. 6 and 7. The potential and vortical contributions to the normal force and their longitudinal loading are decomposed from these pressure measurements by a procedure outlined below.

First, the longitudinal normal loading and the normal force coefficients are obtained by numerical integration of the pressure difference between the lower and upper surfaces of the wing:

$$C_n(\bar{x}) = 2\int_0^1 (C_p^l - C_p^u)\,\frac{s(\bar{x})}{s(1)}\,\mathrm{d}\bar{y} \tag{4}$$

and

$$C_N = \int_0^1 C_n(\bar{x})\,\mathrm{d}\bar{x} \tag{5}$$

Next, the contribution of the attached flow (or potential flow, as denoted by Polhamus[1]) to the longitudinal loading of the normal force, $C_{np}(\bar{x})$, and to the normal force itself, C_{NP}, is deduced from the pressure measurements by invoking the small-perturbation potential-flow wing theory. This is the same theory used in the derivation of $C_{np}(\bar{x})$ and C_{NP} in the LESA method for a wing of zero thickness. The experimental determination of $C_{np}(\bar{x})$ and C_{NP} must be based on the pressures on the lower surface, since this is the only surface on which the flow is attached. On this surface, the pressures contain the contribution of the wing thickness, in addition to the sought contribution of the attached flow. The thickness effects can be isolated from the contribution to $C_{np}(x)$ and C_{NP} by invoking the superposition principle, which is consistent with the small-perturbation potential-flow wing theory. For a wing of zero camber (as is the case with the present wing models), these effects are determined from pressure measurements at $\alpha = 0$ deg. Thus, the pressure contribution of the lower surface to C_{NP} is given by

$$[C_p^l]_{np} = C_p^l - C_{p0}^l \tag{6}$$

The pressure contribution of the upper surface is determined by invoking a result of the linearized potential-flow wing theory, which states that, in the absence of wing thickness and camber, $[C_p^u]_{np}$ is given by

$$[C_p^u]_{np} = -[C_p^l]_{np} \tag{7}$$

$C_{np}(\bar{x})$ and C_{NP} are obtained by numerical integration:

$$C_{np} = 2\int_0^1 \{[C_p^l]_{np} - [C_p^u]_{np}\}\frac{s(\bar{x})}{s(1)}\,d\bar{y}$$

$$= 4\int_0^1 (C_p^l - C_{p0}^l)\frac{s(\bar{x})}{s(1)}\,d\bar{y} \tag{8}$$

and

$$C_{NP} = \int_0^1 C_{np}\,d\bar{x} \tag{9}$$

$C_{nv}(\bar{x})$ and C_{NV} are determined by subtracting the potential component from the normal force:

$$C_{nv}(\bar{x}) = C_n(\bar{x}) - C_{np}(\bar{x}) \tag{10}$$

and

$$C_{NV} = C_N - C_{NP} \tag{11}$$

Thus, the computation of C_{NP} and C_{NV} and their chordwise loadings requires the pressures on the lower surface at the given incidence angle and at $\alpha = 0$ deg.

Results and Discussion

The values of C_{NP}, C_{NV}, and their chordwise distribution were determined experimentally for the two wings. The angle-of-attack range in which these results are given contains the region where LESA is considered applicable and extends beyond the angles of attack at which C_N attains its maximum value.

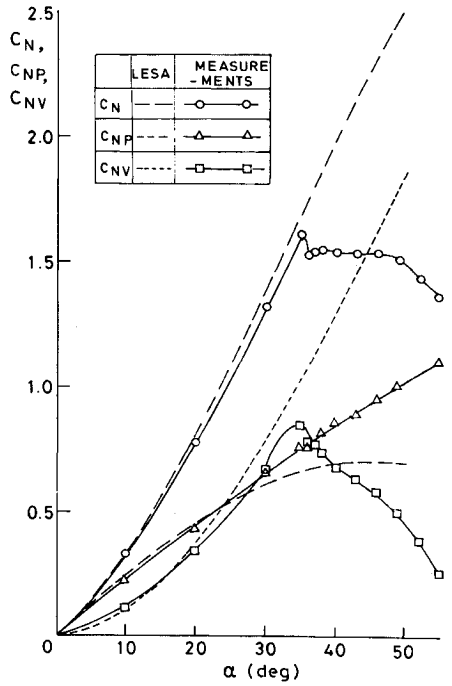

Fig. 4 Measured and predicted values of C_N and its potential and vortical components for the 75-deg sweep delta wing.

Low-Aspect-Ratio Wing

For the low-aspect-ratio wing (Fig. 4), the $C_{NP}(\alpha)$ curve obtained analytically exhibits characteristics similar to the experimental curve. In both cases, C_{NP} increases with incidence at a decreasing slope. There is good agreement between the measured values and the predicted results in the 0 to 20-deg incidence range, whereas at higher angles, the predicted values are lower than the experimental results.

The analytical and experimental $C_{NV}(\alpha)$ curves have similar characteristics in the incidence range of 0–34 deg. In this range, C_{NV} increases with incidence angles at an increasing slope. At higher angles of attack, the analytically determined C_{NV} increases further with the incidence angle, whereas the experimentally determined coefficient exhibits stall-like characteristics and decreases with incidence. The departure of the experimental results from the predicted values is due to the effect of vortex breakdown on the leading-edge vortices. In this aspect ratio, the departure occurs at the incidence angle in which vortex breakdown appears at the trailing edge.[4]

The predicted and experimental curves of $C_N(\alpha)$—the sum of C_{NP} and C_{NV} [Eq. (1)]—have similar characteristics in the prestall angle-of-attack range. The agreement between the experimental and calculated values is good up to 20 deg, as was also previously observed by Polhamus.[1] This agreement is a consequence of the good agreement in the C_{NP} and C_{NV} values in the 0–20-deg range. At higher angles of attack, the predicted C_N values are higher, and the characteristics of the C_N curves are similar to those observed in the C_{NV} curves.

Figures 5 and 6 feature the normalized C_{np} and C_{nv} chordwise loadings, respectively. The measured loadings are given for $\alpha = 20$ and 30 deg along with the predicted results.

Examination of Fig. 5 shows that the measured normalized C_{np} values for the two angles approximately coincide into one curve. This curve is in good agreement with the predicted one, although the latter overestimates the loading in the wing forward section and underestimates it in the trailing-edge region.

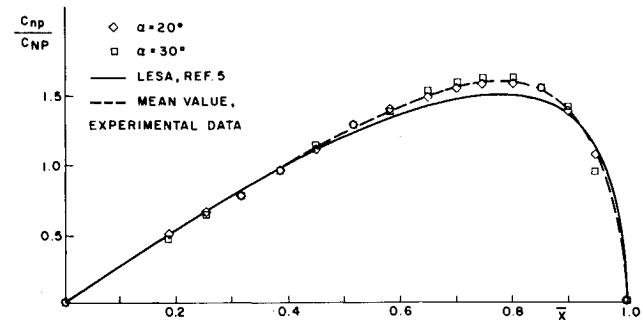

Fig. 5 Measured and predicted C_{np} loading for the 75-deg sweep delta wing.

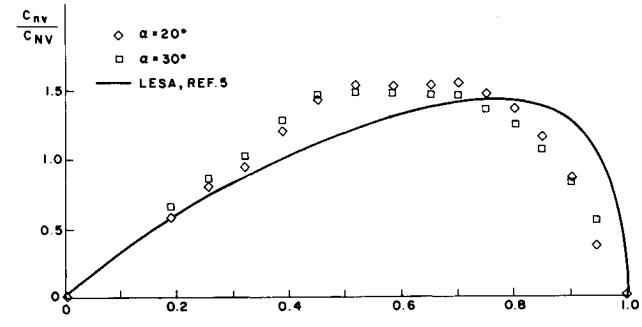

Fig. 6 Measured and predicted C_{nv} loading for the 75-deg sweep delta wing.

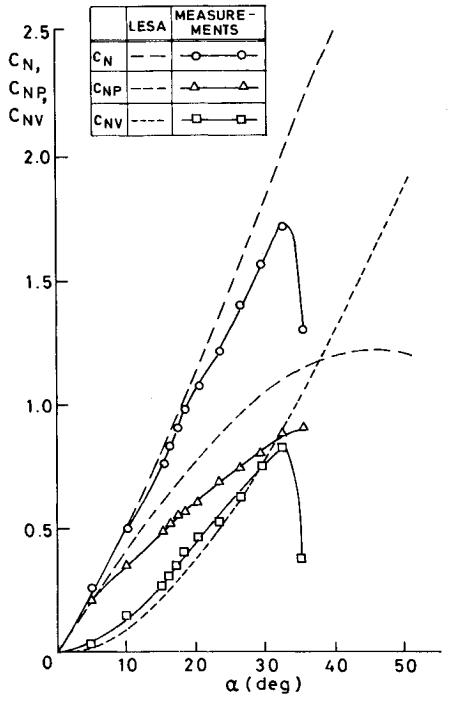

Fig. 7 Experimental and predicted values of C_N and its potential and vortical components for the 60-deg sweep delta wing.

Examination of two measured C_{nv} loadings (Fig. 6) shows that they are in good correlation, as was also the case for C_{np} (Fig. 5). However, the agreement between the measured and predicted results is not as good as that observed in Fig. 5. Here, LESA overestimates the loading in the wing midsection and underestimates it in the aft section. This indicates that the effect of the Kutta condition on the suction generated by the vortices is more pronounced than predicted by LESA.

High-Aspect-Ratio Wing

The characteristic features in the $C_{NP}(\alpha)$, $C_{NV}(\alpha)$, and $C_N(\alpha)$ curves of the high-aspect-ratio wing (Fig. 7) are similar to those observed in the respective curves of the low-aspect-ratio wing (Fig. 4). There are, however, two principal differences.

First, the agreement between the predicted and experimental values of C_N, C_{NP}, and C_{NV} in the incidence range of 0–20 deg is not as good as that observed in the low-aspect-ratio wing. Although the difference between the predicted and experimental values of C_N (in the high-aspect-ratio wing) is relatively small in this range, the corresponding differences in C_{NP} and C_{NV} are considerably larger. At $\alpha \simeq 15$ deg, for example, the predicted value of C_{NP} is higher by approximately 0.10, and that of C_{NV} is lower by approximately 0.05. The normalized differences (with respect to the local measured coefficient) are 20.5% for C_{NP} and −20.0% for C_{NV}. In comparison, the predicted value of C_N is higher than the experimental result by 0.05, and the normalized difference is 6.3%.

The second difference is evident in the characteristics of C_{NV}. In this wing, the maximum value of C_{NV} is attained at $\alpha \simeq 32$ deg—the angle of attack in which vortex breakdown has reached the wing apex.[4]

Figures 8 and 9 feature the normalized chordwise C_{np} and C_{nv} longitudinal loadings, respectively. The measured loadings are shown for $\alpha = 10$ and 15 deg—both angles in the range where the measured and predicted $C_N(\alpha)$ curves are in reasonable agreement, and the effect of vortex breakdown (which appears at the trailing edge at $\alpha \cong 14$ deg) on the upper-surface loading is null at $\alpha = 10$ deg or marginal at $\alpha = 15$ deg.

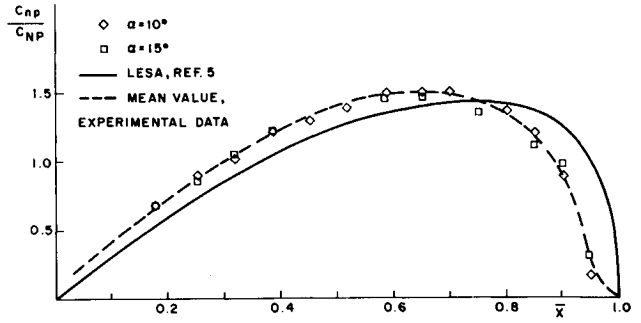

Fig. 8 Measured and predicted C_{np} values for the 60-deg swept wing.

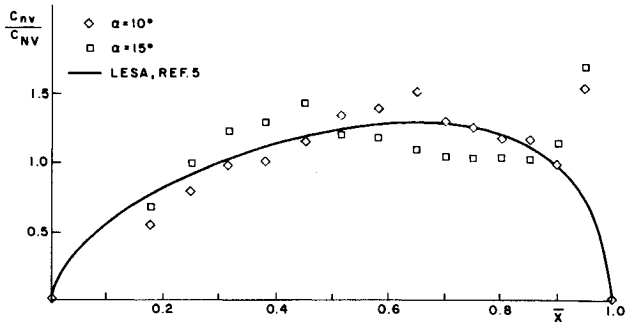

Fig. 9 Measured and predicted C_{nv} values for the 60-deg swept wing.

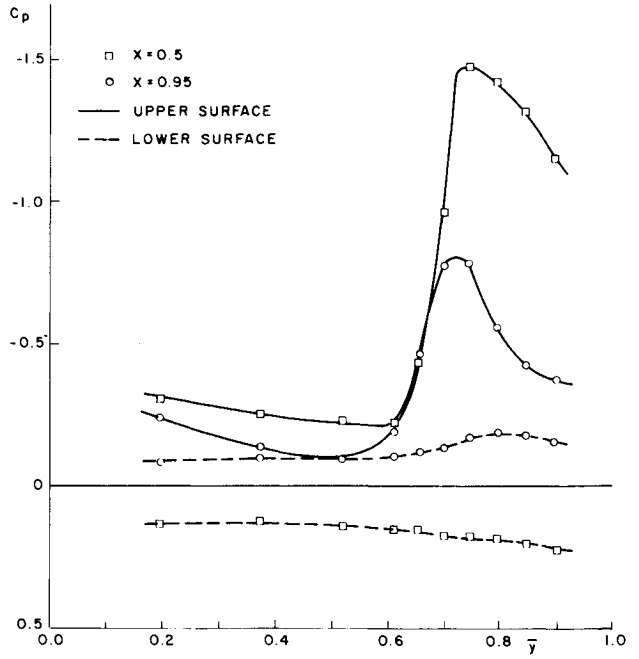

Fig. 10 Spanwise C_p profiles in the 60-deg swept wing for $\kappa = 10$ deg at $\bar{x} = 0.5$ and 0.95.

Examination of the longitudinal C_{np} loadings (Fig. 8) shows that, similar to the low-aspect-ratio wing (Fig. 5), the two normalized measured loadings approximately coincide. However, comparison of the measured and predicted results shows that the agreement is not as good as that observed in Fig. 5. Here, LESA underestimates the effect of the Kutta condition on C_{np}. Attention is drawn to the fact that the measured estimates of C_{np} and $dC_{np}/d\bar{x}$ at $\bar{x} = 0.95$ are considerably lower than those obtained by an interpolation based on the C_{np} values at $\bar{x} = 0.9$ and 1. The reasons for this

difference are evident in Fig. 10, which features the surface pressure distributions for $\alpha = 10$ at $\bar{x} = 0.95$ and 0.5. The first station is the closest one to the trailing edge at which measurements were taken, whereas the second one is located far from the trailing edge and its effects. The two upper-surface profiles have similar characteristics: They are negative throughout with suction peaks induced by the leading-edge vortices. The two lower-surface profiles, however, have different characteristics: at $\bar{x} = 0.5$, the C_p^l values are positive throughout, as is typical to pressure-side results, whereas at $\bar{x} = 0.95$ the C_p^l values are negative. In addition, the latter profile has a small peak underneath the one on the upper surface. This indicates that, for this wing, the suction on the upper surface "leaks" into the lower surface at the trailing-edge region. This leakage is manifested in the negative C_{np} values at $\bar{x} = 0.95$.

For the C_{nv} loading (Fig. 9), the correlation between the measured results at $\alpha = 10$ and 15 deg is less good than that observed in C_{np} for the same wing or in C_{nv} of the low-aspect-ratio wing. In addition, the agreement between measured and predicted results is not good. The differences are strongly evident at the trailing-edge region and, in particular, at $\bar{x} = 0.95$, where the measured values are considerably higher than the predicted ones. The latter result is a consequence of the fact that C_{nv} is obtained by subtracting C_{np} from C_n [Eq. (10)] and that C_{np} has a lower than "expected" value of $\bar{x} = 0.95$ due to the trailing-edge effect shown in Fig. 10.

Conclusions

The potential and vortical contributions to the normal force, as well as the normal force itself, as predicted by the Leading-Edge Suction Analogy (LESA), were compared with results deduced from experimental data. Since both LESA and the method presented here are based on a small-perturbation potential-flow theory, the comparison can, in principle, be valid only for low angles of attack.

A quantitative comparison shows that, in the low-aspect-ratio wing, there is good agreement between experiment and theory in the C_N values, as well as for the C_{NP} and C_{NV} components in the 0–20 deg incidence range. The agreement in the C_{nv} and C_{np} loadings is also good up to $\alpha = 30$ deg, although it is less than that observed in the integral coefficients. In the high-aspect-ratio wing, the agreement between the measured and predicted C_N values is good up to $\alpha \simeq 10$ deg, and a relatively small difference appears at higher incidence angles. This latter agreement, however, is not evident in the C_{NP} and C_{NV} values, where considerably larger differences are observed. However, these differences are such that when C_{NP} and C_{NV} are summed, to produce C_N, the differences tend to cancel each other out. Consequently, the normalized difference in C_N for this wing is smaller than in the C_{NP} and C_{NV} components. The large differences are also observed in the C_{nv} and C_{np} loadings. Thus, LESA appears less valid for the high-aspect-ratio wing than was previously thought on the basis of a comparison of just the C_N values.

In the incidence range beyond that, where the quantitative agreement is good, there is still qualitative agreement up to the angle of stall. Vortex breakdown, which is the cause of this stall, has a stronger effect on the low-aspect-ratio wing, where a sharp decrease in C_{NV} is observed at the angle of attack at which breakdown appears at the trailing edge. In comparison, the stall in the high-aspect-ratio wing occurs when vortex breakdown has reached the apex and the leading-edge vortices are affected by the breakdown throughout almost their entire length.

In summary, this study shows that LESA provides good predictions of not just the normal force, but also of its potential and vortical components, as well as its longitudinal loadings. Care should be taken when applying this analogy to wings having aspect ratios larger than 2.

References

[1]Polhamus, E. C., "A Concept of the Vortex Lift of Sharp Edge Delta Wings Based on a Leading-Edge Suction Analogy," NASA TN D-3767, Dec. 1966.

[2]Polhamus, E. C., "Prediction of Vortex-Lift Characteristics by a Leading-Edge Suction Analogy," *Journal of Aircraft*, Vol. 8, April 1971, pp. 193–199.

[3]Polhamus, E. C., "Charts for Predicting the Subsonic Vortex Lift Characteristics of Arrow, Delta and Diamond Wings," NASA TN D-6243, April 1971.

[4]Wentz, W. H. Jr. and Kohlman, D. L., "Wind Tunnel Investigations of Vortex Breakdown on Slender Sharp-Edged Wings," Univ. of Kansas Center of Research, Lawrence, KS, Rept. FRL 69-013, Nov. 1968.

[5]Synder, M. H. and Lamar, J. E., "Application of the Leading-Edge Suction Analogy to Prediction of Longitudinal Load Distribution and Pitching Moments for Sharp-Edged Delta Wings," NASA TN D-6994, Oct. 1972.

[6]Zohar, Y., "The Effects of Vortex Breakdown on the Aerodynamic Characteristics of Delta Wings," M.Sc. thesis, Technion, Israel, 1984.

[7]Er-El, J. and Weihs, D., "Ground Effect on Delta Wings at Moderate and High Angles of Attack," ICAS Paper 84-2.8.3, *Proceedings of the 14th ICAS Congress*, Toulouse, France, Sept. 1984, pp. 896–904.